

## Electronic Supplementary Information (ESI)

### **Integrating multiple adsorption sites and tortuous diffusion path into a metal-organic framework for C<sub>3</sub>H<sub>4</sub>/C<sub>3</sub>H<sub>6</sub> separation**

Xue-Qian Wu,<sup>a</sup> Yabo Xie,<sup>a</sup> Jing-Hao Liu,<sup>b</sup> Tao He,<sup>a</sup> Yong-Zheng Zhang,<sup>a</sup> Jiamei Yu,<sup>b</sup>  
Xiang-Jing Kong,<sup>a</sup> Jian-Rong Li\*,<sup>a</sup>

<sup>a</sup> *Beijing Key Laboratory for Green Catalysis and Separation and Department of Chemistry and Chemical Engineering, College of Environmental and Energy Engineering, Beijing University of Technology, Beijing 100124, P. R. China.*

<sup>b</sup> *College of Materials Science and Engineering, Beijing University of Technology, Beijing 100124, P. R. China*

#### **Materials and Methods**

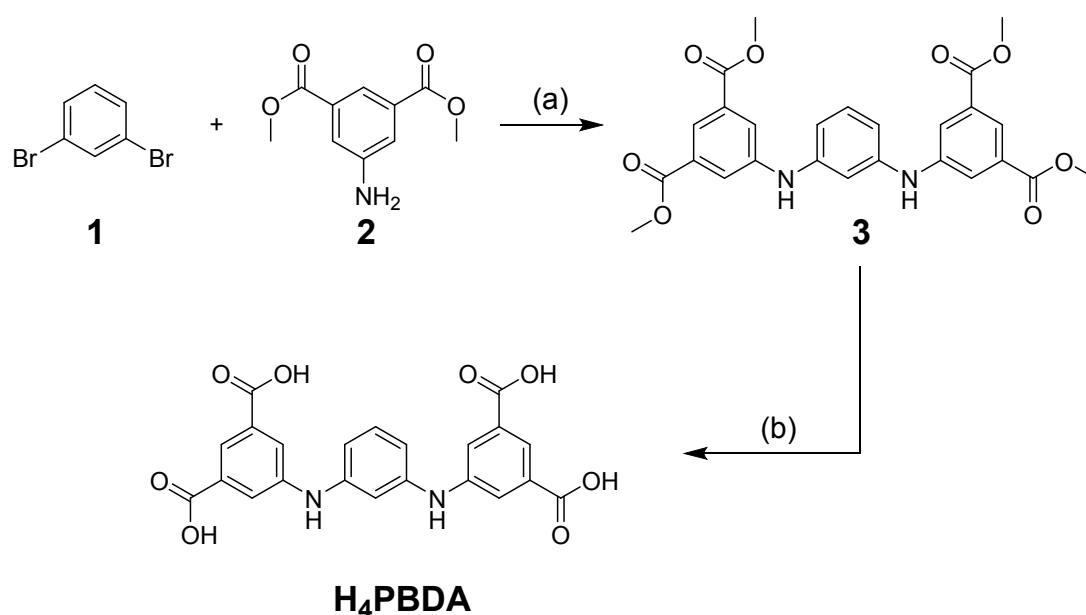
All the reagents (AR grade) were purchased from commercial sources and used directly without any further purification. Powder X-ray diffraction (PXRD) data were recorded on a Bruker D8-Focus Bragg-Brentano X-ray powder diffractometer equipped with a Cu sealed tube ( $\lambda = 1.54178 \text{ \AA}$ ) at room temperature (RT). <sup>1</sup>H NMR data were collected on a Bruker Avance III HD 400 MHz NMR spectrometer. Thermogravimetric (TG) curve was obtained on a TGA-50 thermogravimetric analyzer with a heating rate of 10 °C min<sup>-1</sup> under air atmosphere. Fourier-transform infrared (FT-IR) spectra were recorded on an IR Affinity-1 instrument. Gas adsorption experiments were carried out through a Micrometrics ASAP 2020 surface area and pore analyzer. Kinetic adsorption were measured with the Intelligent Gravimetric Analyzer (IGA001, Hiden, UK), which uses a gravimetric technique to accurately measure the gas sorption.

## Synthesis and characterization of H<sub>4</sub>PBDA ligand

As shown in scheme S1, the organic ligand was synthesized on a two steps procedure including N-C coupling and hydrolysis reaction:<sup>1</sup>

### Synthesis of **3**

To the mixture of 1,3-dibromobenzene (5.0 g, 21.2 mmol), dimethyl 5-aminoisophthalate (10.6 g, 50.8 mmol), K<sub>2</sub>CO<sub>3</sub> (8.2 g, 59.3 mmol) in H<sub>2</sub>O (0.09 mL) and *t*-BuOH (250 mL) under N<sub>2</sub> atmosphere, Pd(OAc)<sub>2</sub> (0.28 g, 1.3 mmol) and *t*BuXPhos (1.6 g, 3.9 mmol) were added. The reaction mixture was stirred at 110 °C for 24 h. After cooling to room temperature, water (250 mL) was added to the mixture and tetramethyl 5,5'-(1,3-phenylenebis(azanediyl))diisophthalate (**3**, 8.5 g, 81%) was isolated as white solid. <sup>1</sup>H NMR (CDCl<sub>3</sub>, 400 MHz): δ = 8.21 (s, 2H), 7.91 (s, 4H), 7.26-7.28 (m, 1H), 6.79-6.81 (m, 3H), 6.01 (s, 2H), 3.94 (s, 12H).



**Scheme S1.** The synthesis of ligand H<sub>4</sub>PBDA: (a) K<sub>2</sub>CO<sub>3</sub>, Pd(OAc)<sub>2</sub>, *t*BuXPhos, H<sub>2</sub>O/*t*-BuOH, N<sub>2</sub> atmosphere, 110 °C for 24 h; (b) NaOH, THF/MeOH/H<sub>2</sub>O, 70 °C, 24 h.

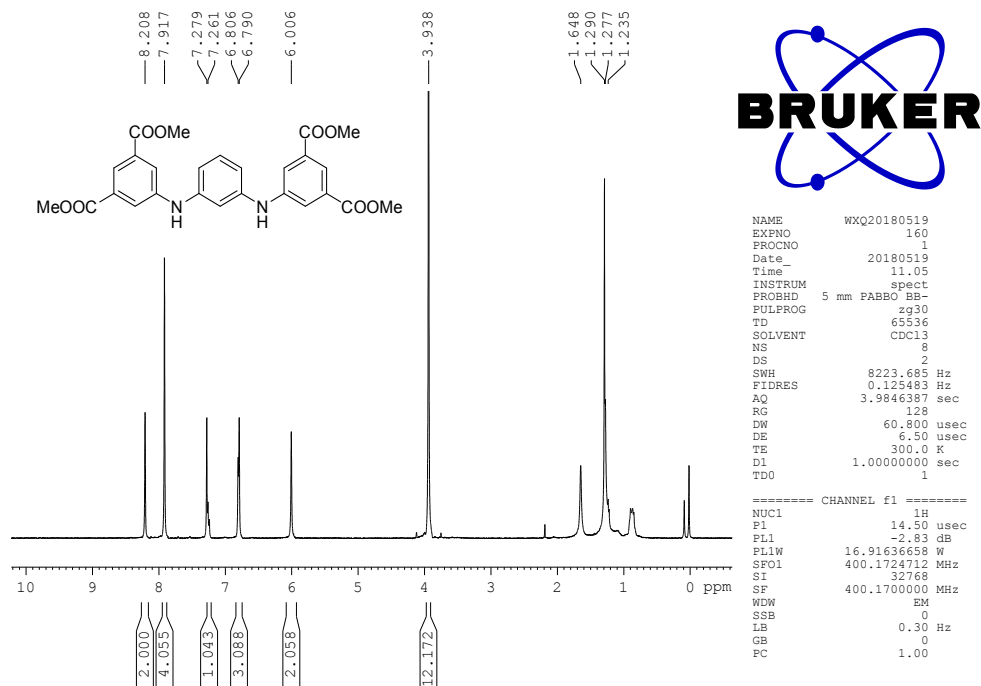


**Fig. S1.** The  $^1\text{H}$  NMR spectrum of **3**.

### Synthesis of $\text{H}_4\text{PBDA}$

**3** (8.5 g, 17.3 mmol) and NaOH (4.1 g, 103.6 mmol) in THF (100 mL), MeOH (100 mL) and  $\text{H}_2\text{O}$  (100 mL) were stirred at 70 °C for 24 h. After completion of the reaction, organic solvents were removed in vacuum. The filtrate was acidized with 1 M HCl to pH = 5, to give yellow precipitate. The resulting precipitate was centrifuged, washed with water, and dried at 60 °C in vacuum to give  $\text{H}_4\text{PBDA}$  as yellow solid (5.8 g, 77%).  $^1\text{H}$  NMR ( $\text{DMSO-}d_6$ , 400 MHz):  $\delta$  = 13.11 (s, 4H), 8.60 (s, 2H), 7.91 (s, 2H), 7.84 (s, 4H), 7.25 (t,  $J$  = 8.0 Hz, 1H), 6.83 (s, 1H), 7.46 (d,  $J$  = 8.0 Hz, 2H).

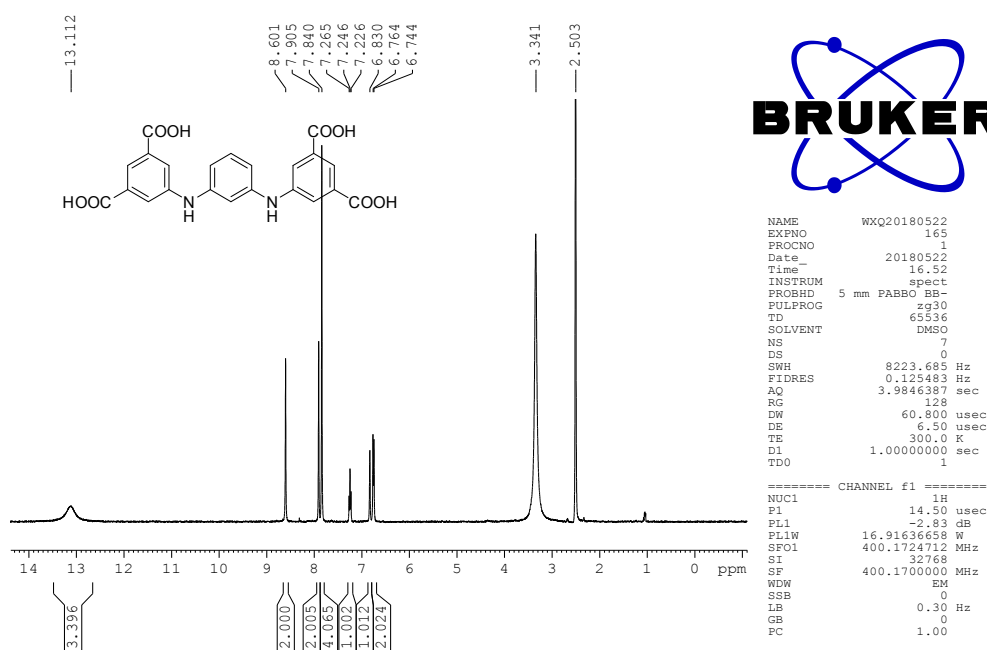


**Fig. S2.** The <sup>1</sup>H NMR spectrum of H<sub>4</sub>PBDA.

### Synthesis of [Cu<sub>12</sub>(PBDA)<sub>4</sub>(DABCO)<sub>3</sub>(COO)<sub>8</sub>(H<sub>2</sub>O)<sub>6</sub>] $\cdot$ xS (BUT-310)

A mixture of Cu(NO<sub>3</sub>)<sub>2</sub>·2.5H<sub>2</sub>O (20 mg, 0.086 mmol), H<sub>4</sub>PBDA (15 mg, 0.034 mmol), 1,4-diazabicyclo[2.2.2]-octane (DABCO) (10 mg, 0.089 mmol), DMF (5 mL), ethanol (3 mL), H<sub>2</sub>O (2.5 mL) and 200 μL of HBF<sub>4</sub> were added to a 20 mL vial; then, the vial was transferred to an oven and heated at 65 °C for 12 h. Dark green crystals were collected, washed with DMF, and air dried (85% yield based on Cu(NO<sub>3</sub>)<sub>2</sub>·2.5 H<sub>2</sub>O). The experimental and simulated PXRD patterns are well matched, indicating that the as-prepared sample is obtained as the pure phase (Fig. S3).

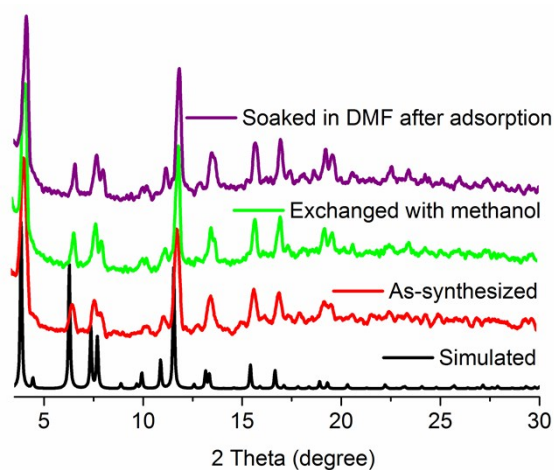


**Fig. S3.** The PXRD patterns of as-synthesized BUT-310 (red) and BUT-310 samples after adsorption (purple) and exchanged with methanol (green).

### Single Crystal X-ray Structure Determination

The diffraction data of as-synthesized BUT-310 was collected in an Rigaku Supernova CCD diffractometer equipped with a mirror monochromated enhanced Cu- $K\alpha$  radiation ( $\lambda = 1.54184 \text{ \AA}$ ) at 298 K. The structure was solved by ShelXT solution program with the intrinsic phasing method and refined by full-matrix least-squares on  $F^2$  with anisotropic displacement using the SHELXTL and Olex2 software package.<sup>2</sup> Hydrogen atoms of ligands were calculated in ideal positions with isotropic displacement parameters. Those in the coordinated water and disordered DABCO were not added but were considered in the final molecular formula. Partial C, N atoms in the structure were disordered and treated by occupancies refinement. The guest molecules were highly disordered and could not be modeled properly, the residual electron densities resulting from them were removed by the SQUEEZE routine in PLATON and the details were appended in the CIF file. The final formula of BUT-310 was calculated from crystallographic data combined with thermogravimetric analysis data. Crystallographic data for BUT-310 has been deposited in Cambridge Crystallographic Data Centre (CCDC number: 1921372). The topologies of BUT-310 was calculated with TOPOS 4.0.<sup>3</sup> Selected crystal parameters and structure refinements are summarized in the following Table S1 and Table S2.

**Table S1.** Crystal data and structure refinement for the BUT-310.

Formula	Cu <sub>48</sub> C <sub>456</sub> H <sub>448</sub> O <sub>216</sub> N <sub>56</sub>
Formula weight	13232
Temperature (K)	293(2)
Crystal system	cubic
Space group	<i>Fm-3m</i>
<i>a</i> / Å	39.7902(6)
<i>b</i> / Å	39.7902(6)
<i>c</i> / Å	39.7902(6)
$\alpha$ /°	90
$\beta$ /°	90
$\gamma$ /°	90
<i>V</i> / Å <sup>3</sup>	62998(3)
<i>Z</i>	2
<i>D</i> <sub>calcd</sub> /g cm <sup>-3</sup>	0.676
$\mu$ /mm <sup>-1</sup>	1.201
Reflections collected	11870
Independent reflections	3109
Goodness-of-fit on <i>F</i> <sup>2</sup>	1.042
<sup>a</sup> <i>R</i> <sub>1</sub> ( <i>I</i> > 2σ( <i>I</i> ))	0.0815
<sup>a</sup> <i>R</i> <sub>1</sub> (all data)	0.1007

$$^a R_1 = \sum ||F_o| - |F_c|| / \sum |F_o|.$$

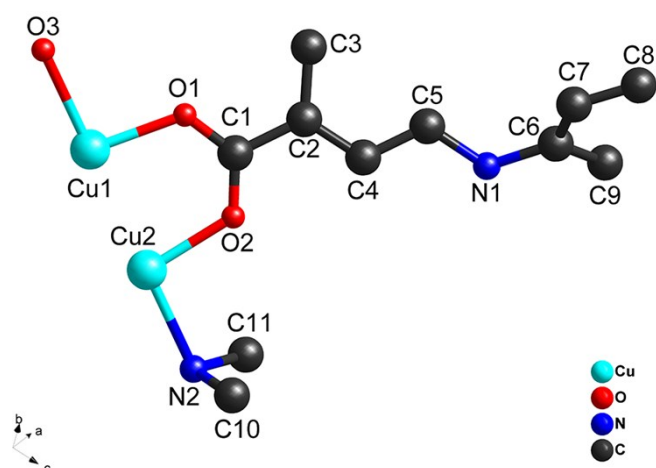


**Fig. S4.** Diagram showing the asymmetric unit of BUT-310 (H atoms are omitted for clarity).

**Table S2.** Selected atomic coordinate and *occupancy information* (disordered and thereby *defect forming*) of BUT-310 obtained from single crystal diffraction data.

atom	x	y	z	occupancy
Cu1	0.5000	0.31147(2)	0.68853(2)	1.0000
Cu2	0.5000	0.35830(2)	0.64170(2)	1.0000
N1	0.6250(3)	0.3750(3)	0.7904(3)	0.6667
N2	0.5000	0.27297(11)	0.72703(11)	1.0000
O1	0.53461(8)	0.37926(8)	0.66934(8)	1.0000
O2	0.53474(9)	0.33976(9)	0.70908(9)	1.0000
O3	0.5000	0.39703(16)	0.60297(16)	1.0000
C1	0.54561(12)	0.36585(12)	0.69580(14)	1.0000
C2	0.57387(13)	0.38319(14)	0.71322(15)	0.6667
C3	0.58896(13)	0.41104(13)	0.69803(19)	0.6667
C4	0.58613(19)	0.3716(2)	0.7435(2)	0.6667
C5	0.6131(3)	0.3869(3)	0.7594(3)	0.6667
C6	0.6428(6)	0.3956(7)	0.8145(5)	0.3333
C7	0.6379(6)	0.4286(8)	0.8208(6)	0.3333
C8	0.6580(8)	0.4438(13)	0.8420(8)	0.3333
C9	0.6704(7)	0.3771(11)	0.8296(7)	0.3333
C10	0.4855(5)	0.2855(4)	0.7578(4)	0.3333
C11	0.5367(4)	0.2655(3)	0.7345(3)	0.6667

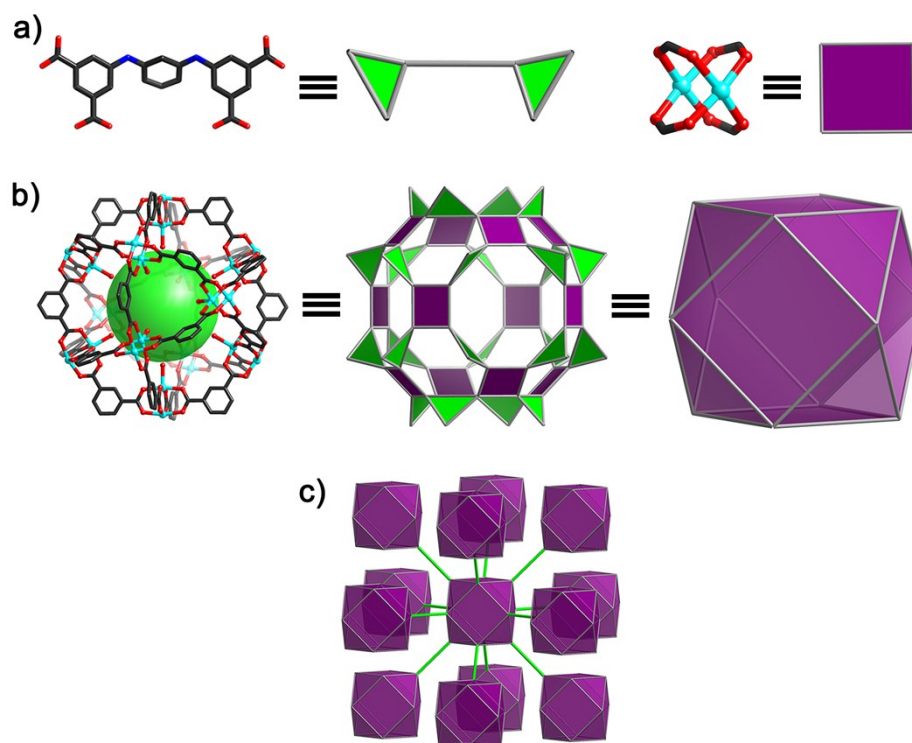


**Fig. S5.** a, b) Ligand PBDA<sup>4-</sup>, Cu (II) paddlewheel SBU and MOP polyhedron represents different nodes, respectively, and c) the **fcu** topology for BUT-310.

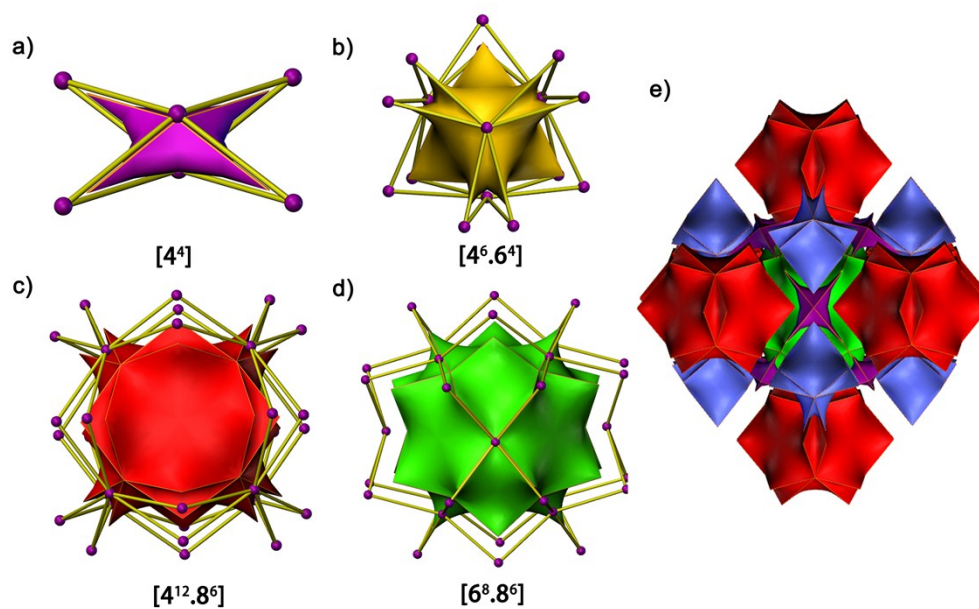


**Fig. S6.** (a-d) Four types of tiles with face symbol and (e) the natural tiling of BUT-310.

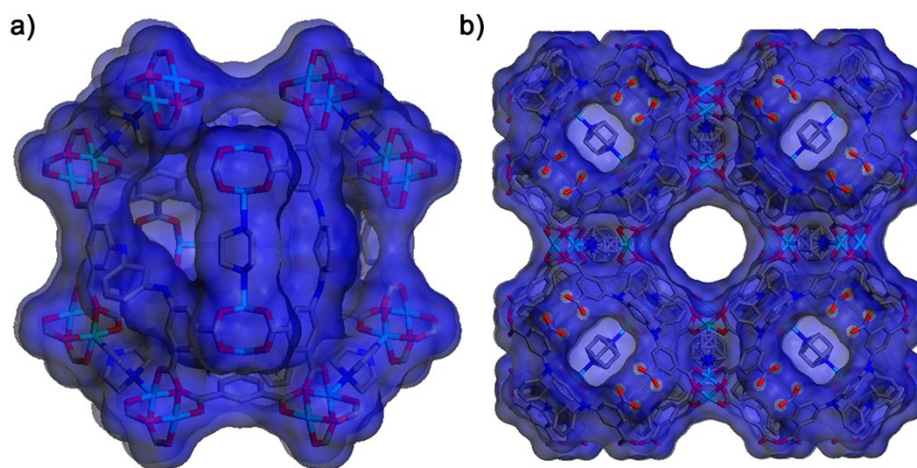


**Fig. S7.** (a, b) Connolly surface representation of BUT-310 (probe radius = 1.8 Å) showing two kinds of diffusion paths within the framework.

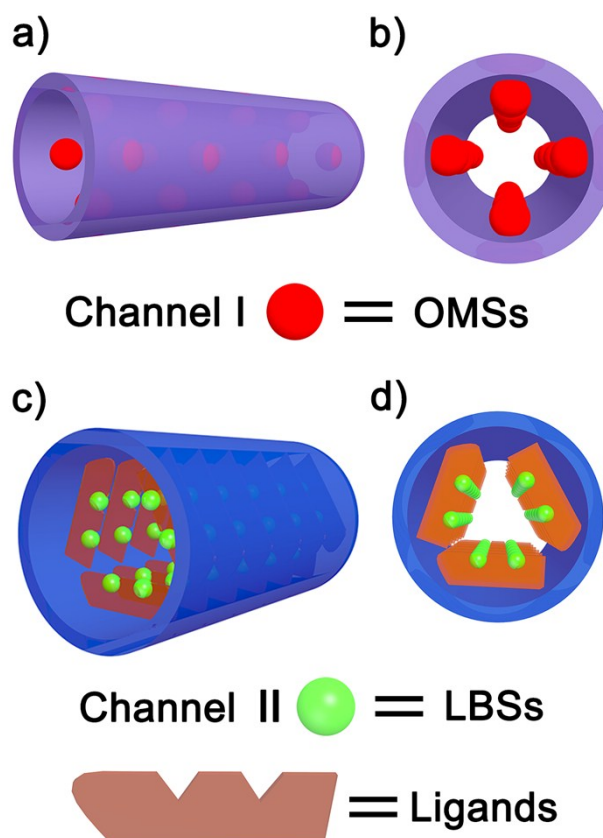


**Fig. S8.** Schematic illustration of the two kinds of diffusion paths within BUT-310. From the crystallographic structure of BUT-310, the open metal sites (OMSs) are mainly distributed on the inner surface of the “channel I” while Lewis basic sites (LBSs) produce efficacy with “channel II”.

### Sample activation and gas adsorption

Before gas adsorption measurements, about 120 mg crystalline samples of BUT-310 were soaked in 20 mL of DMF for 24 h at room temperature. The samples were then soaked in 15 mL of methanol for 48 h and finally transferred into dichloromethane (10 mL) for another 12 h (fresh solvents were changed every 8 h). After solvent exchange, the samples were loaded in a sample tube and further activated under high vacuum at an optimized temperature of 80 °C for 6 h. Eventually, the gas adsorption tests were performed at 77 K in a liquid nitrogen bath, 273 K (an ice-water bath) and 298 K (a water bath). All the gases used were of 99.999% purity.

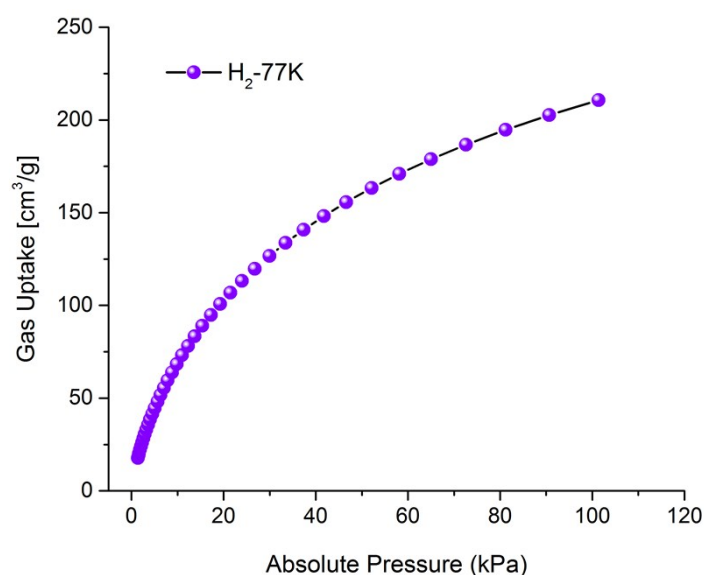


**Fig. S9.** H<sub>2</sub> adsorption isotherm of BUT-310 at 77 K.

### FT-IR spectra of BUT-310

The FT-IR spectra of BUT-310 are available in Fig. S9. As can be seen from the spectra, the stretching vibration absorption peak of the carboxyl groups in H<sub>4</sub>PBDA is at 1720 cm<sup>-1</sup>. After these carboxyl groups are involved in coordination, their characteristic peaks appear at 1691 cm<sup>-1</sup>. Besides, a sharp absorption peak around 3343 cm<sup>-1</sup> should be contributed to the vibration behavior of R<sub>2</sub>-NH group.

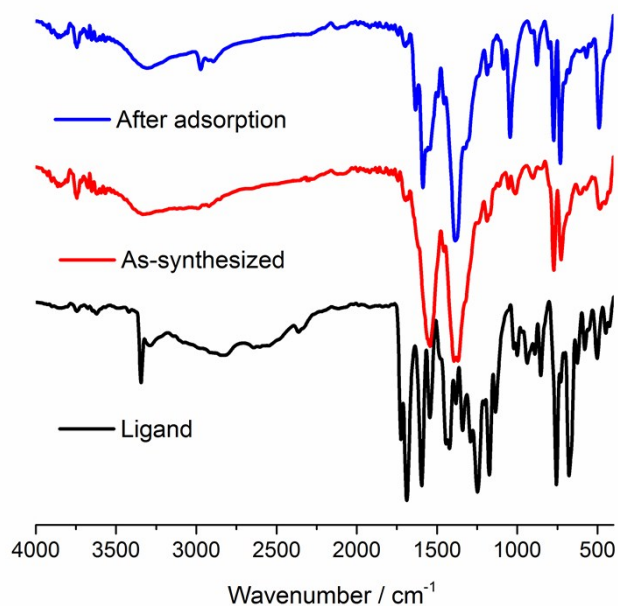


**Fig. S10.** FT-IR spectra of BUT-310 and the ligand.

### TGA curves of BUT-310

To evaluate the thermal stability of BUT-310, TGA analyses were conducted in the temperature range of 30-800 °C and the results are displayed in Fig. S10. The activated BUT-310 shows the first mass loss of 15.9% before 174 °C due to the removal of guest water and coordinated water molecules (mainly derived from the environment before test). The second step exhibits a weight loss of 58.5% from 254 to 433 °C, indicating the decomposition of H<sub>4</sub>PBDA, HCOOH and DABCO ligand. For the freshly prepared BUT-310 sample, a continuous weight lossing process was observed in the temperature range of 30-360 °C, which can be attributed to the removal of a large amount of guest solvent molecules (DMF/H<sub>2</sub>O) and the coordinated water. The next decomposition step is similar to that of the activated sample.

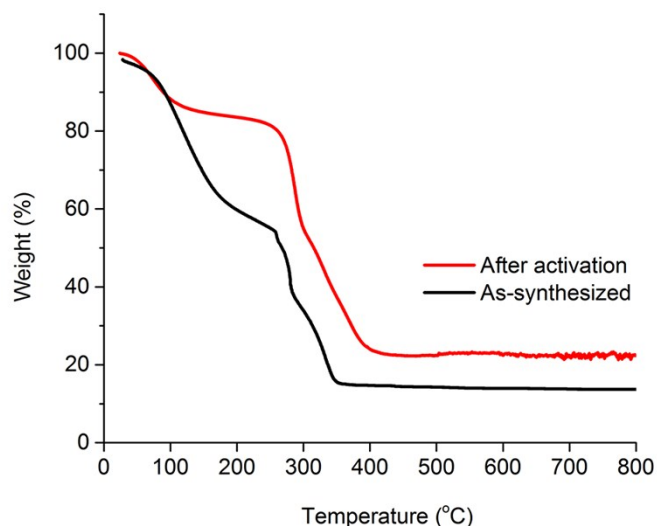


**Fig. S11.** TGA curves of activated BUT-310 and freshly prepared BUT-310.

### Scanning electron microscopy (SEM)

The morphological feature of BUT-310 sample was inspected with a SEM (SU 3500) method. As presented in Fig. S11, the size of the polyhedral-like crystals is about 10-20  $\mu\text{m}$ .

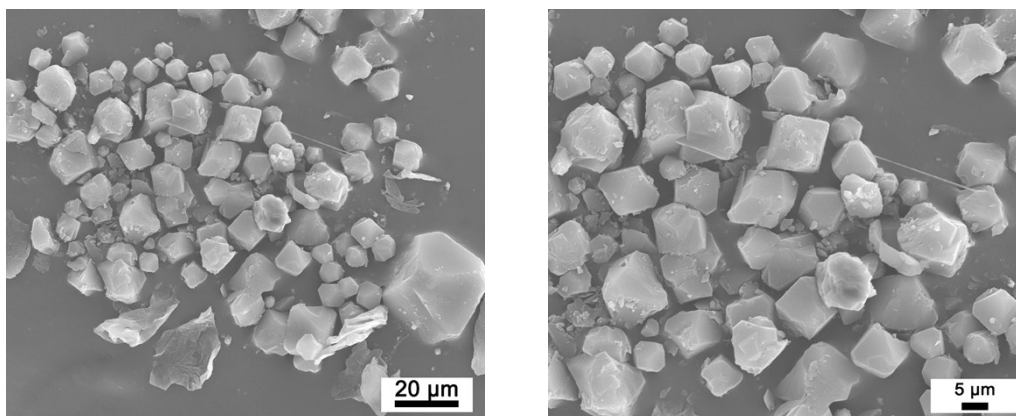


**Fig. S12.** SEM images of BUT-310 crystals.

### Calculation of isosteric heat of adsorption

In order to evaluate the bonding energy between  $\text{C}_3\text{H}_4/\text{C}_3\text{H}_6$  and BUT-310, the isosteric heat of adsorption were calculated according to the following equation:<sup>4</sup>

$$Q_{\text{st}} = -R \sum_{i=0}^m a_i N^i \quad (1)$$

$$\ln P = \ln N + \frac{1}{T} \sum_{i=0}^m a_i N^i + \sum_{j=0}^n b_j N^j \quad (2)$$

A virial-type expression of above equation comprising the temperature-independent parameters  $a_i$  and  $b_j$  was employed to calculate the enthalpies of adsorption for  $C_3H_4/C_3H_6$  at 273 K and 298 K on BUT-310. Where  $P$  is the pressure (mmHg),  $T$  is the temperature (K),  $a_i$  and  $b_j$  are virial coefficients,  $N$  is the adsorption amount in mg/g and the  $m/n$  represents the number of coefficients used to describe the adsorption curves.  $Q_{st}$  is coverage-dependent enthalpy of adsorption and  $R$  is the universal gas constant.

### Calculation procedures of selectivity from IAST

Ideal adsorbed solution theory (IAST) enables prediction of adsorption equilibriums of the binary gas mixtures from the related single-component isotherms.<sup>5</sup> The single-site Langmuir-Freundlich equation and dual-site Langmuir-Freundlich equation were used for fitting the adsorption data at 298 K.

$$N = A_1 \times \frac{b_1 P^{C_1}}{1 + b_1 P^{C_1}} + A_2 \times \frac{b_2 P^{C_2}}{1 + b_2 P^{C_2}} \quad (3) \quad (A_2 = 0, \text{ single-site model})$$

Here  $N$  is the adsorption amount in  $cm^3/g$ ,  $P$  is the pressure of the bulk gas at equilibrium with the adsorbed phase (bar),  $A_1$  and  $A_2$  are the saturation loadings of sites A and B ( $cm^3/g$ ),  $b_1$  and  $b_2$  are the affinity coefficients of sites A and B (1/bar),  $C_1$  and  $C_2$  represent the deviations from an ideal homogeneous surface. The fitting parameters of the equation (3) for  $C_3H_4$  and  $C_3H_6$  are listed in the table (insert: Fig. S12). These parameters were applied to perform the next calculation:

$$S_{1,2} = \frac{q_1 / p_1}{q_2 / p_2} \quad (4)$$

$q_1$  and  $q_2$  are the equilibrated adsorption molar loading of component 1 and 2 respectively,  $p_1$  and  $p_2$  represent the partial pressure of component 1 and 2 in bulk gas phase.

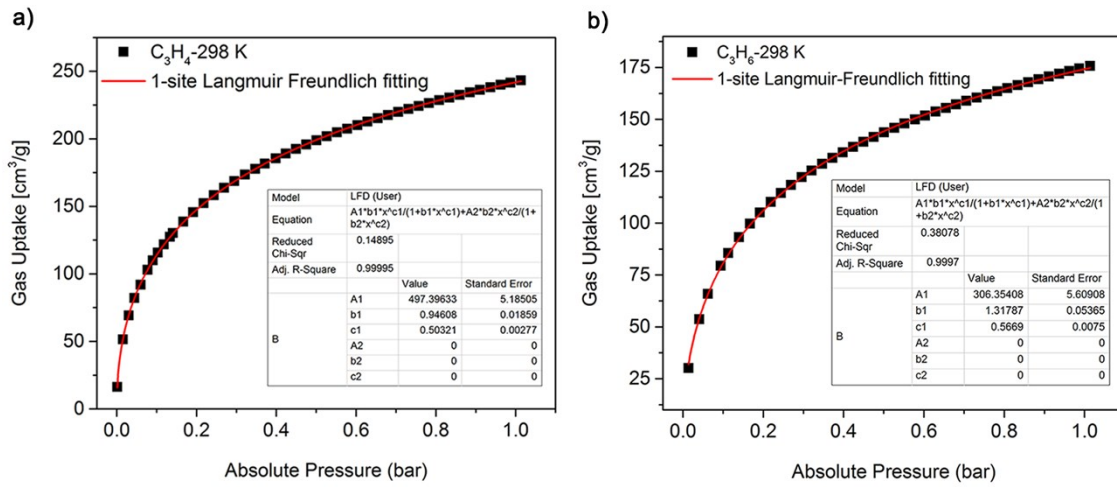


**Fig. S13.**  $C_3H_4$  and  $C_3H_6$  adsorption isotherms at 298 K in BUT-310 with single-site Langmuir-Freundlich model fit.

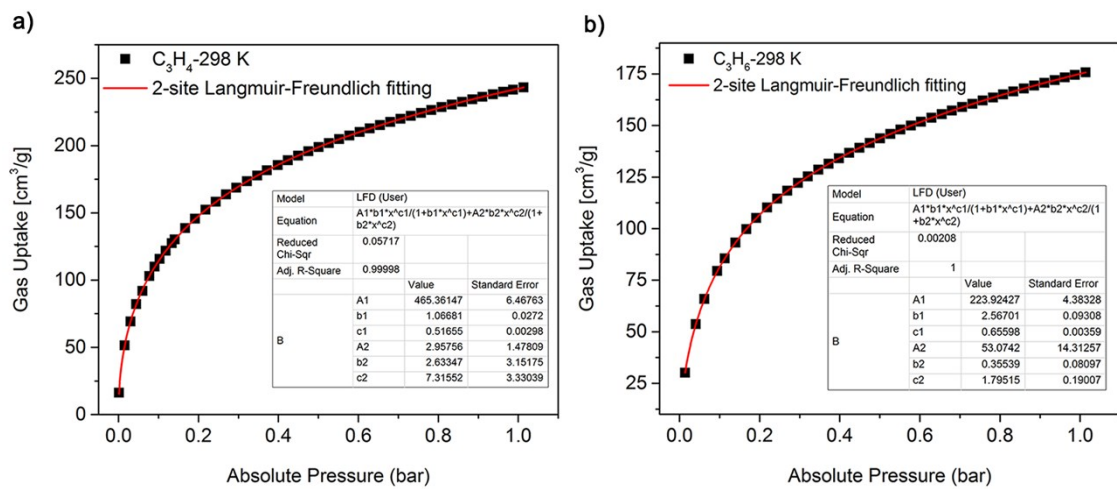


**Fig. S14.**  $C_3H_4$  and  $C_3H_6$  adsorption isotherms at 298 K in BUT-310 with dual-site Langmuir-Freundlich model fit.

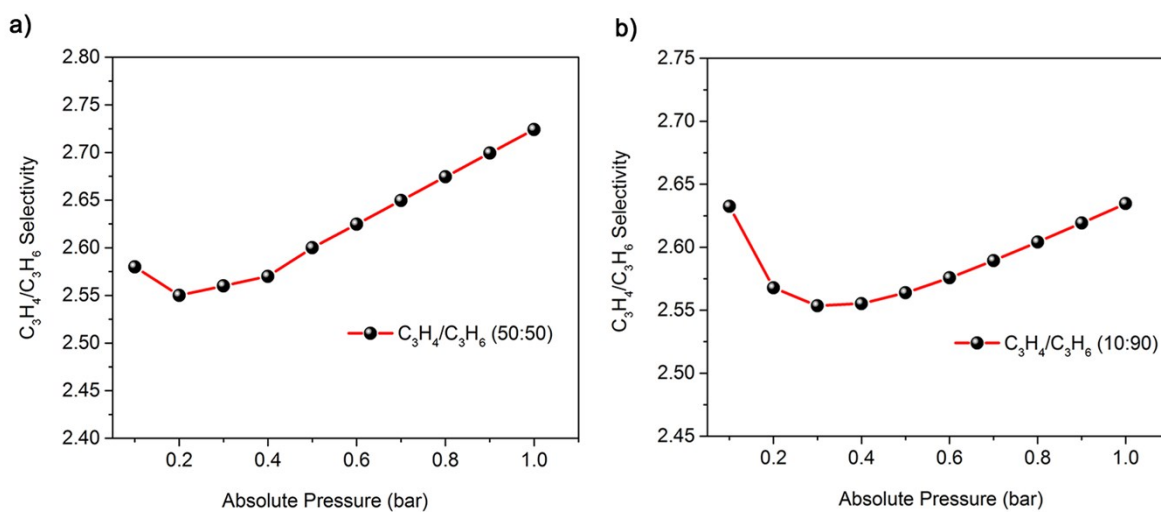


**Fig. S15.** IAST selectivity of BUT-310 for  $C_3H_4/C_3H_6$  (a: 50:50; b: 10:90) at 1 bar, 298 K.

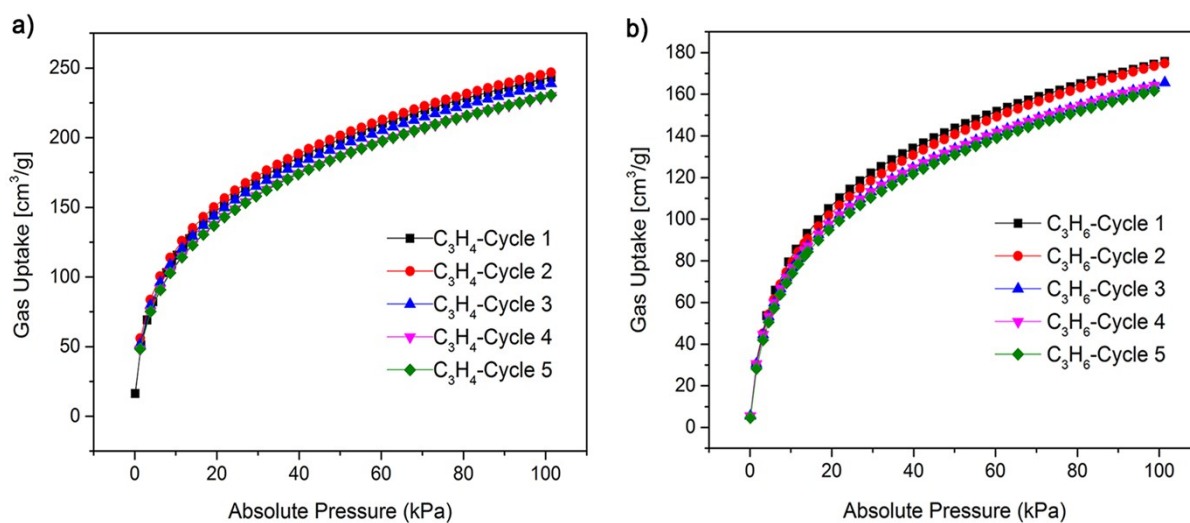


**Fig. S16.** Cyclic  $C_3H_4$  and  $C_3H_6$  adsorption measurements in BUT-310 at 298 K, indicating that BUT-310 can maintain its high  $C_3H_4$  and  $C_3H_6$  uptake capacities over five cycles.

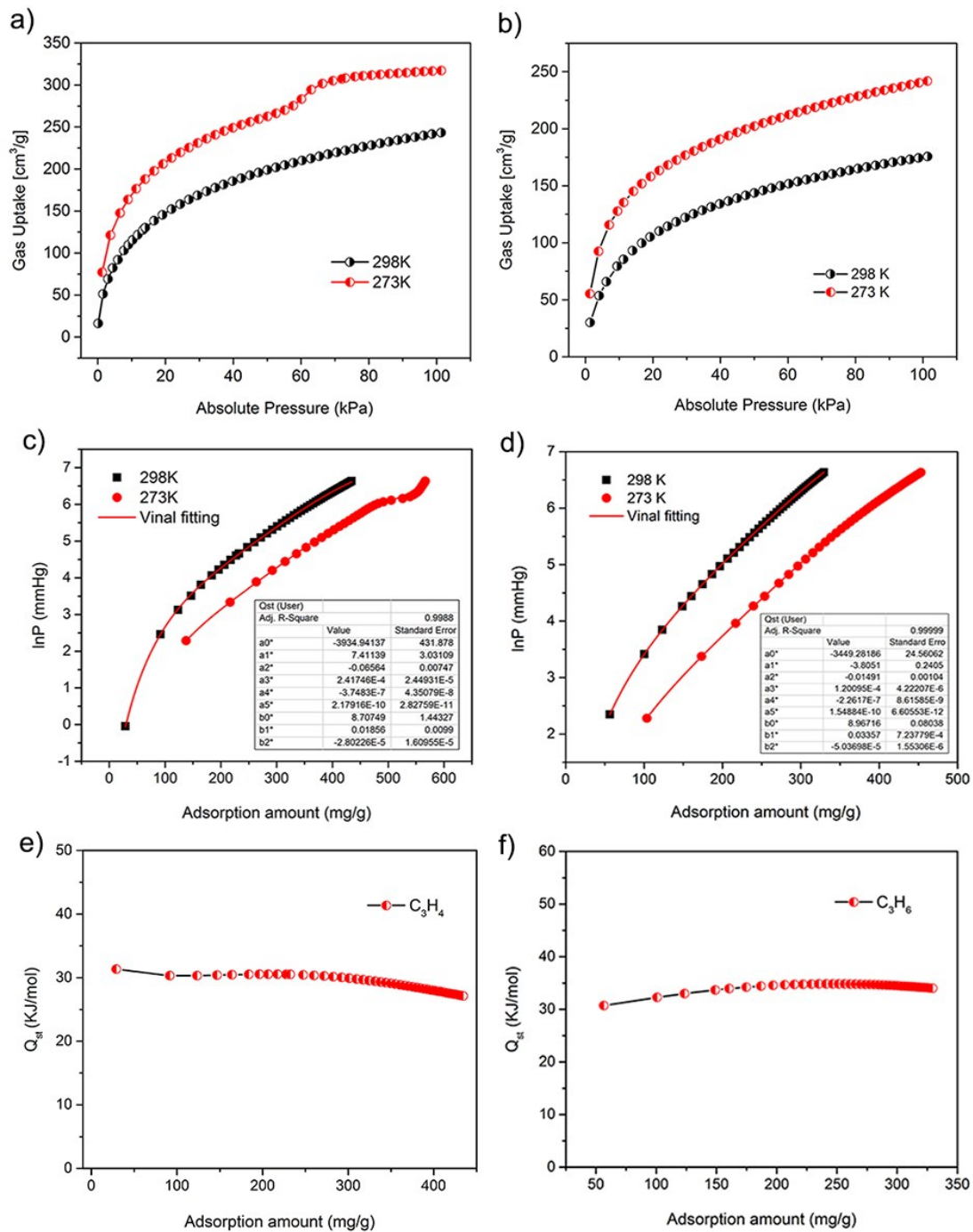


**Fig. S17.** Adsorption isotherms of (a)  $C_3H_4$  and (b)  $C_3H_6$  in BUT-310 at 298 K and 273 K. (c) Virial fitting of  $C_3H_4$  and (d)  $C_3H_6$  adsorption isotherms for  $Q_{st}$  calculation. The related fitting parameters are also listed in the picture (insert). (e), (f) Isosteric heat of adsorption of  $C_3H_4$  and (b)  $C_3H_6$  in BUT-310.

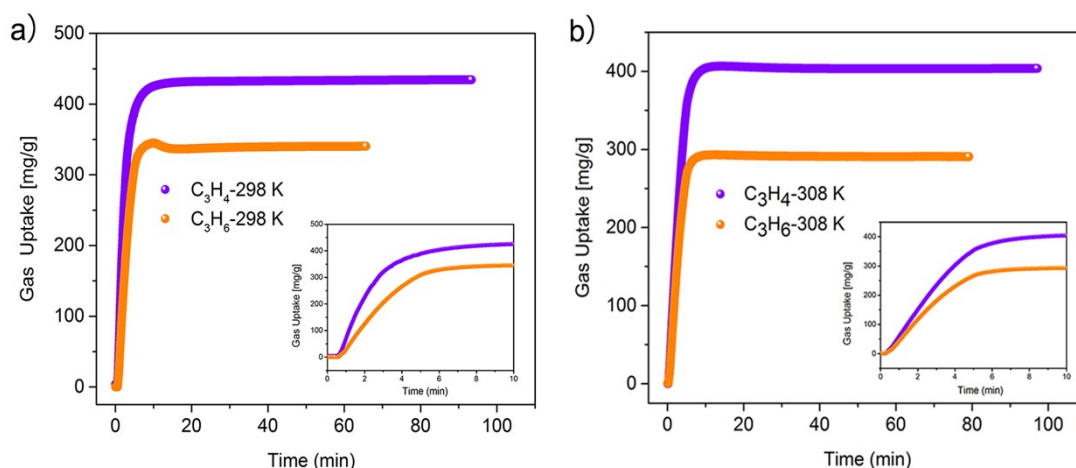


**Fig. S18.** Isotherms of the relationship between the adsorption amount and the equilibrium time (a: 298 K, b: 308 K).

### Grand Canonical Monte Carlo simulations

The Grand Canonical Monte Carlo simulations (GCMC) were performed for C<sub>3</sub>H<sub>4</sub> and C<sub>3</sub>H<sub>6</sub> adsorption on BUT-310 at 100 kPa and 298 K (or 0.1-100 kPa, 298 K). The gas molecules and MOF skeleton were both treated as rigid bodies. The dispersive and steric repulsive interactions of the each atoms in BUT-310 framework and C<sub>3</sub>H<sub>4</sub>/C<sub>3</sub>H<sub>6</sub> adsorbates were both modeled by the dreiding force field (Dreiding) or universal force field (UFF), which have been widely applied in the simulation for MOFs.<sup>6</sup> The related Lennard-Jones parameters for the framework and gas molecules were listed in table S3. The QEq method was used to equilibrate and redistribute the overall charge of atoms of the MOF structure, while the charge distribution situation for C<sub>3</sub>H<sub>4</sub>/C<sub>3</sub>H<sub>6</sub> molecules was calculated through DFT (ESP). The schematic illustration of the partial charges on C<sub>3</sub>H<sub>4</sub>/C<sub>3</sub>H<sub>6</sub> atoms was given in Fig. S19. Electrostatic interaction was evaluated through Ewald summation method. The cutoff distance was set at 18.5 Å. 20000000 Monte Carle steps were constructed to simulate the favorable adsorption sites, adsorption isotherms and the saturation uptakes under a fixed pressure, in which the first 10000000 steps were for equilibration and the remains were production steps. Fugacity was calculated from the Peng-Robinson

equation of state.<sup>7</sup> All the simulations were carried out by using sorption/DMol3 module in the Material Studio software.<sup>8</sup> Most of the LJ parameters were taken from Dreiding force field apart copper, for which LJ parameters were gain from Universal Force Field (UFF).

**Table S3.** Force field parameters for the BUT-310 and C<sub>3</sub>H<sub>4</sub>/C<sub>3</sub>H<sub>6</sub> taken from the Dreiding and Universal Force Field (UFF)

Element	Force field	$\sigma$ (Å)	$\epsilon/k_B$ (K)
C <sub>3</sub> H <sub>4</sub> -C ( <i>sp</i> <sup>3</sup> )	Dreiding	3.70	125.80
C <sub>3</sub> H <sub>4</sub> -C ( <i>sp</i> )	Dreiding	3.47	47.85
C <sub>3</sub> H <sub>4</sub> -C ( <i>sp</i> )	Dreiding	3.55	73.82
C <sub>3</sub> H <sub>6</sub> -C ( <i>sp</i> <sup>2</sup> )	Dreiding	3.47	47.85
C <sub>3</sub> H <sub>6</sub> -C ( <i>sp</i> <sup>3</sup> )	Dreiding	3.47	47.85
MOF-C ( <i>sp</i> <sup>2</sup> )	Dreiding	3.47	47.85
MOF-C ( <i>sp</i> <sup>3</sup> )	Dreiding	3.47	47.85
N	Dreiding	3.26	38.95
O	Dreiding	3.03	48.16
H	Dreiding	2.85	7.65
Cu	UFF	3.11	2.52
Qe		0	0

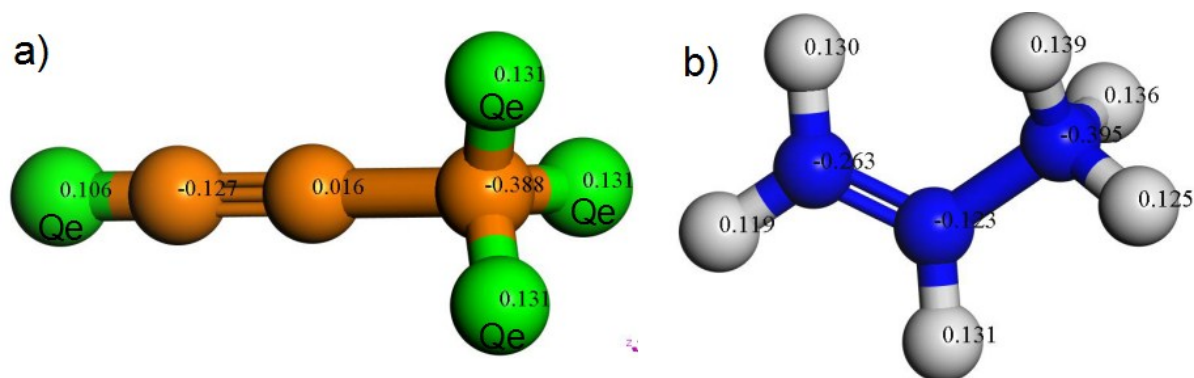


**Fig. S19** Schematic representation of the models and charge distributions for the gas adsorbates (a: C<sub>3</sub>H<sub>4</sub>, b: C<sub>3</sub>H<sub>6</sub>).

In order to validate the accuracy of the force fields (Dreiding and UFF), the simulations were firstly performed for C<sub>3</sub>H<sub>4</sub> and C<sub>3</sub>H<sub>6</sub> adsorption on BUT-310 at 100 kPa and 298 K. According to the experimental data, the C<sub>3</sub>H<sub>4</sub> and C<sub>3</sub>H<sub>6</sub> uptake capacity in BUT-310 is 243 cm<sup>3</sup> g<sup>-1</sup> and 175.7 cm<sup>3</sup> g<sup>-1</sup>, respectively. The theoretical loading amounts of C<sub>3</sub>H<sub>4</sub> and C<sub>3</sub>H<sub>6</sub> in BUT-310 were calculated to be 249.8 cm<sup>3</sup> g<sup>-1</sup> (C<sub>3</sub>H<sub>4</sub>) and 183.9 cm<sup>3</sup> g<sup>-1</sup> (C<sub>3</sub>H<sub>6</sub>), confirming the suitability of the force fields for gas adsorbates and framework. Meanwhile, the simulated C<sub>3</sub>H<sub>4</sub>/C<sub>3</sub>H<sub>6</sub> adsorption isotherms agree well with the experimental results, which further supported the suitability of the force fields. It should be pointed out that the theoretical adsorption capacities of C<sub>3</sub>H<sub>4</sub>/C<sub>3</sub>H<sub>6</sub> in BUT-310 are higher than the related experimental data under some specific pressures. This phenomenon can be attributed to the following factor: the framework of BUT-310 was regarded as perfect crystalline structure during the simulation processes, however, the synthesized sample usually possesses structural defects, especially for highly disordered structure.<sup>9</sup> Furthermore, GCMC simulations were carried out for binary mixtures (50:50) at 100 kPa to verify the validity of the IAST selectivity. The theoretical adsorption capacities of C<sub>3</sub>H<sub>4</sub> and C<sub>3</sub>H<sub>6</sub> are 164.8 cm<sup>3</sup> g<sup>-1</sup> and 54.9 cm<sup>3</sup> g<sup>-1</sup> from GCMC, respectively, and the simulated selectivity of C<sub>3</sub>H<sub>4</sub>/C<sub>3</sub>H<sub>6</sub> was calculated to be 3.0, which is consistent with the IAST selectivity (2.73).

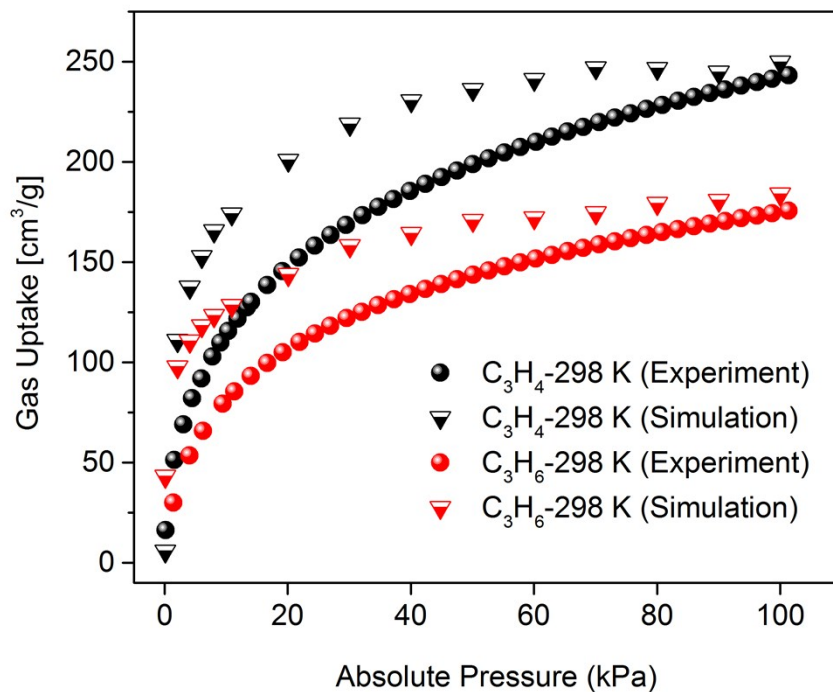


**Fig. S20.** Experimental and simulated  $C_3H_4/C_3H_6$  adsorption isotherms at 298 K.

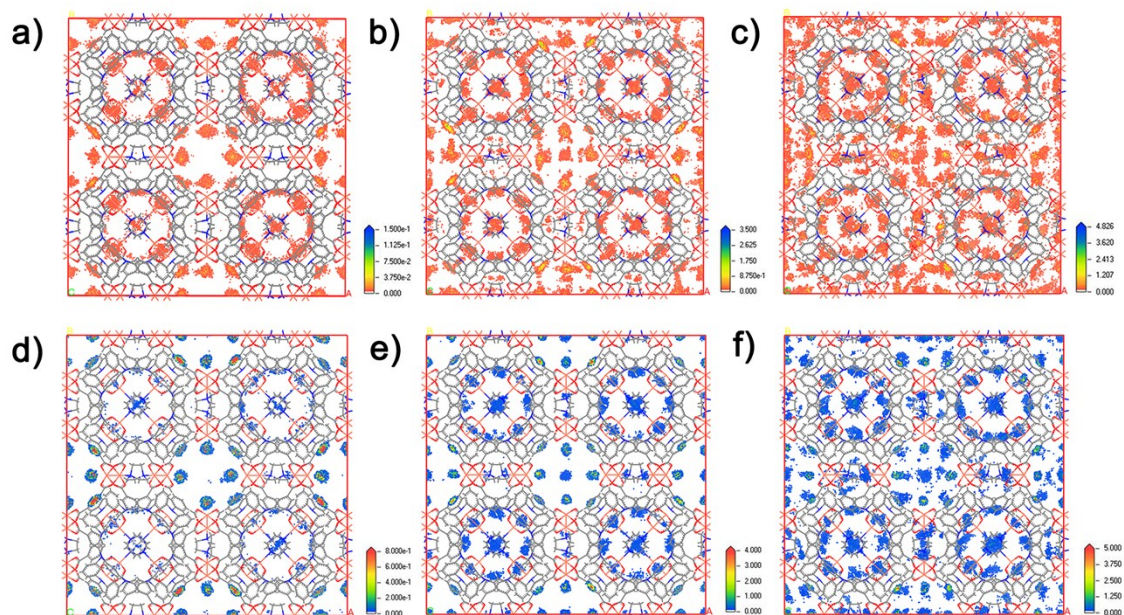


**Fig. S21.** The  $C_3H_4/C_3H_6$  density profiles of at 0.1, 10 and 100 kPa from GCMC simulations.

The simulations at lower pressure were carried out to indicate the uniform and wide distribution of adsorption sites within the framework. As shown in Fig. S21, the

C<sub>3</sub>H<sub>4</sub>/C<sub>3</sub>H<sub>6</sub> molecules are widely distributed around the binding sites even under 0.1 kPa based on the typical cuboctahedral MOP cage and another symmetric cage. After all sites are occupied, the free space becomes filled with gases gradually with the increase of pressure.

### **Molecular dynamics simulations**

Molecular dynamics (MD) simulations were performed using the LAMMPS package<sup>10</sup> in the canonical (NVT) ensemble at 298 K controlled using the Nosé-Hoover thermostat.<sup>11-12</sup> The initial configurations were obtained from GCMC simulation at 100 kPa. We then ran a MD simulation (11.0 ns) and the initial 1.0 ns was discarded for equilibration. Periodic boundary conditions were applied in three directions. The equation of motion was propagated using the velocity Verlet algorithm<sup>13</sup> with a time step of 1.0 fs. The cutoff distance of the non-bonded and Coulomb interactions was set to 1.2 nm. The long-range Coulomb interactions between point charges were handled using the particle-particle particle-mesh (PPPM) method.<sup>14</sup>

The diffusion coefficients were calculated according to the Einstein diffusion equation:

$$D = \frac{1}{2d} \lim_{t \rightarrow \infty} \frac{\langle [r(t) - r(0)]^2 \rangle}{t}$$

Where D is the self-diffusion coefficient, d (taken to be 3) is dimensionality of the system and t is the elapsed time. The numerator is the mean square displacement (MSD) and the angled brackets indicate an ensemble average is to be taken.

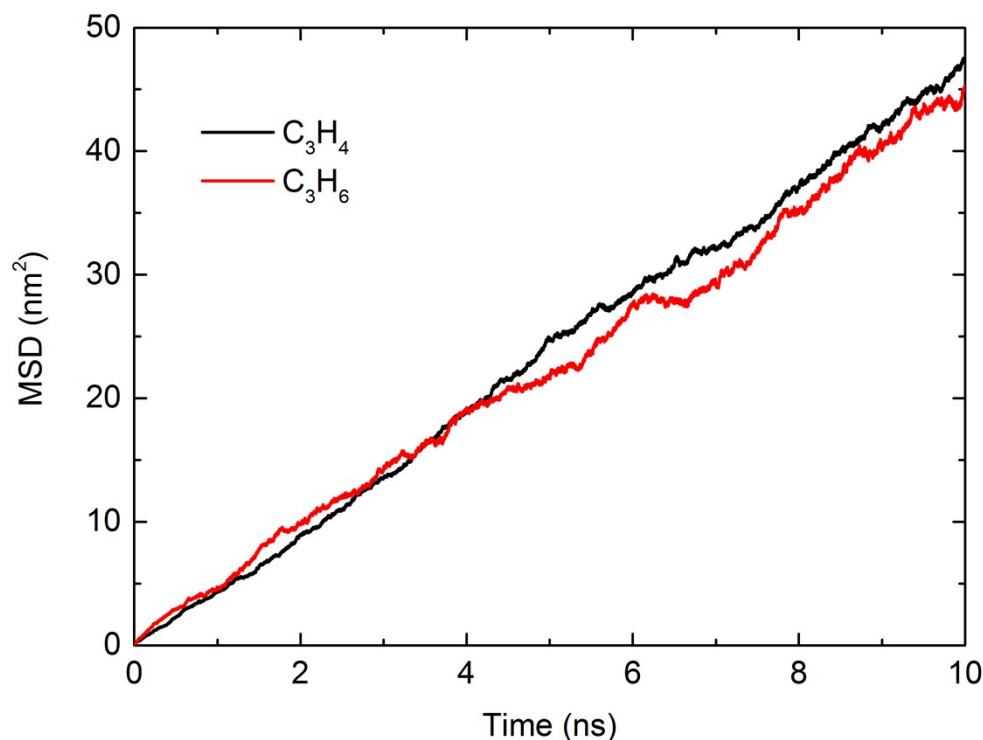


**Fig. S22.** The mean square displacement (MSD) curves for C<sub>3</sub>H<sub>4</sub>/C<sub>3</sub>H<sub>6</sub> from MD simulations.

### Breakthrough experiment

The typical breakthrough device is consisted of five parts: gas cylinder, flow controller, adsorption bed, heating jacket and gas analyzer (Fig. S17).<sup>15</sup> Breakthrough experiments were then carried out in a 4 mm diameter quartz tube of 130 mm length packed with 150 mg of BUT-310 (solvent-exchanged powder sample, particle size 10~20 μm) in which C<sub>3</sub>H<sub>4</sub>/C<sub>3</sub>H<sub>6</sub> gas mixture was flowed with a total flow of 4 mL/min at 298 K and 1.0 bar. The sample was heated at 80 °C for 6 h under a flow of He (20 mL/min) for complete activation before the measurement. The gas compositions at the outlet determined continuously by mass spectrometry (MS, Hiden, HPR-20). After the contents of outlet gas reached the equilibrium, the adsorption bed was regenerated by He flow (20 mL/min) for 4 h at room temperature.

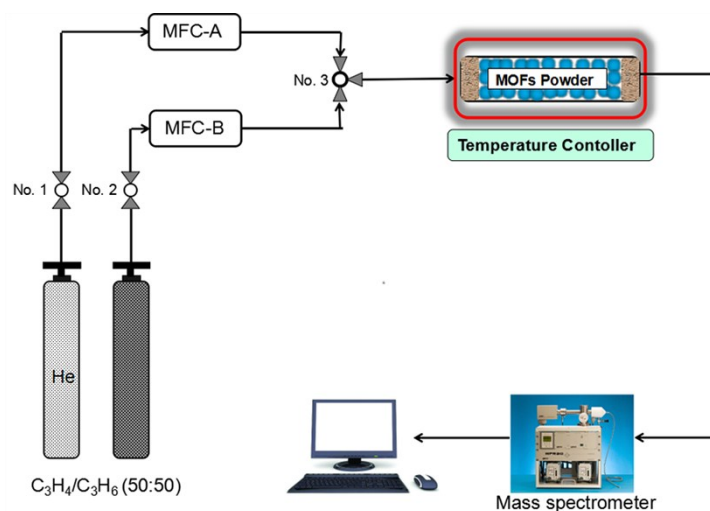


**Fig. S23.** Schematic illustration of the apparatus used for the breakthrough experiment.



**Fig. S24.** The photograph of the packing column used for the breakthrough experiments.

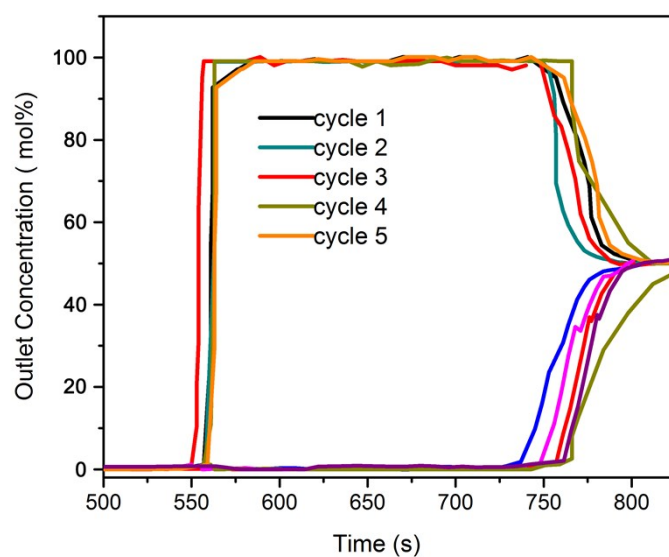


**Fig. S25.** Cyclic  $C_3H_4/C_3H_6$  (50/50) separation experiments in BUT-310 at 298 K, indicating that BUT-310 can maintain its separation abilities over five cycles.

**Table S4.** Numerical gas adsorption data of BUT-310 at 298 K or 273 K

Relative Pressure ( $P/P_0$ )	Gas Uptake ( $\text{cm}^3/\text{g}$ )	Absolute Pressure (kPa)	Gas Uptake ( $\text{cm}^3/\text{g}$ )
<b>N<sub>2</sub> (77 K)</b>		<b>H<sub>2</sub> (77 K)</b>	
2.17E-06	15.15299	1.39228	17.72417
1.65E-06	30.30986	1.54957	19.27076
1.81E-06	45.46707	1.64243	20.18852
2.53E-06	60.62354	1.87174	22.26706
4.28E-06	75.77584	2.07568	24.0253
7.61E-06	90.91726	2.32235	26.08264
1.27E-05	106.04831	2.59845	28.26918
1.98E-05	121.16448	2.89804	30.56627
2.92E-05	136.26086	3.24294	33.07148
4.15E-05	151.33469	3.6187	35.69607
6.08E-05	166.47517	4.04134	38.50435
8.54E-05	181.60842	4.5237	41.53148
1.21E-04	196.73198	5.04283	44.67195
1.77E-04	211.83369	5.64826	48.14261
2.66E-04	226.91238	6.30686	51.73071
4.18E-04	241.9519	7.04755	55.55242
6.60E-04	256.94632	7.86536	59.56245
0.00103	271.86002	8.79119	63.8524
0.00154	286.67421	9.81817	68.32441
0.00222	301.36878	10.99822	73.17803
0.00309	315.96109	12.26988	78.08537
0.00415	330.43266	13.71604	83.34371
0.00542	344.75052	15.39102	89.01459
0.00692	358.92895	17.24008	94.85926
0.00881	373.20673	19.23015	100.72075
0.01119	387.16884	21.4684	106.86133
0.02932	437.76035	23.95995	113.19066
0.05975	475.28188	26.73884	119.76292
0.08462	496.05186	29.93466	126.69569
0.10114	506.32516	33.43799	133.68298
0.12209	517.6239	37.35439	140.85864
0.14198	528.39373	41.74716	148.21056
0.16146	539.81295	46.62456	155.68796
0.17983	553.35122	52.10114	163.32502
0.19863	592.98808	58.12596	170.96773
0.26177	608.93024	64.98563	178.83555
0.33989	615.2406	72.59546	186.71541
0.37413	617.26206	81.20117	194.69154

0.39979	618.56295	90.68267	202.65183
0.44964	620.62811	101.35761	210.71911
0.49993	622.45689		
0.55015	623.92289	<b>Absolute Pressure (kPa)</b>	<b>Gas Uptake (cm<sup>3</sup>/g)</b>
0.59978	625.20817	<b>CH<sub>4</sub> (298 K)</b>	
0.6498	626.31221	6.92182	1.15453
0.69969	627.31537	10.25332	1.70046
0.74984	628.19534	11.57514	1.90704
0.7997	628.96048	14.11859	2.31594
0.81955	629.35904	16.68262	2.7231
0.85004	629.7858	19.24839	3.12819
0.87444	630.15254	21.84684	3.54029
0.89958	630.55876	24.36424	3.92549
0.92474	630.93642	27.2763	4.3771
0.94953	631.28624	29.48608	4.71427
0.9744	631.72933	32.06253	5.10503
0.97957	631.91792	34.97052	5.5431
0.98838	633.46257	37.58501	5.93345
0.99037	639.74867	40.08168	6.31046
		42.6171	6.68783
<b>Absolute Pressure (kPa)</b>	<b>Gas Uptake (cm<sup>3</sup>/g)</b>	45.32238	7.08549
<b>CO<sub>2</sub> (298 K)</b>		47.90142	7.46441
5.63295	3.61348	50.28302	7.81365
8.27311	5.32576	52.86555	8.18529
9.50251	6.09856	55.48795	8.56093
11.56491	7.40295	58.00245	8.92543
13.59857	8.67798	60.53447	9.28747
15.66462	9.94791	63.07514	9.6447
17.62833	11.17641	65.68366	10.01717
19.73966	12.47237	68.3341	10.38813
21.76625	13.7079	70.77294	10.72965
23.81035	14.96731	73.4426	11.10598
25.86324	16.22359	76.00247	11.46013
27.89642	17.4569	78.53842	11.81009
29.93363	18.70062	81.08084	12.16399
31.9799	19.94206	83.61086	12.50501
34.03165	21.18581	86.07293	12.83558
36.05566	22.39927	88.80975	13.20284
38.09049	23.6269	91.35472	13.55448
40.15191	24.8668	93.83096	13.88233
42.15797	26.07542	96.14901	14.2005

44.23502	27.29893	98.908	14.56646
46.24811	28.48952	101.55078	14.91754
48.28121	29.69097		
50.33768	30.89816	<b>Absolute Pressure (kPa)</b>	<b>Gas Uptake (cm<sup>3</sup>/g)</b>
52.38471	32.10046	<b>C<sub>2</sub>H<sub>2</sub> (298 K)</b>	
54.41959	33.27159	3.81788	12.63704
56.46096	34.44634	4.32797	14.00006
58.49859	35.61732	4.95523	15.62998
60.52602	36.77661	5.98871	18.16099
62.57465	37.94172	7.00123	20.51589
64.60665	39.09549	8.00396	22.73528
66.64951	40.24562	9.00353	24.86209
68.69437	41.38292	10.00897	26.88169
70.73941	42.51436	15.07484	35.98867
72.77562	43.62585	20.03552	43.62777
74.82216	44.72823	24.97209	50.16511
76.84764	45.82076	29.94045	56.04806
78.89048	46.91543	34.97906	61.44116
80.93758	48.01097	39.9834	66.34158
82.97648	49.08855	44.98226	70.92326
84.99956	50.16164	50.00011	75.21597
87.04121	51.23902	54.99274	79.23104
89.09077	52.29881	59.98152	83.07263
91.11529	53.34871	64.99874	86.77235
93.15805	54.39594	69.99395	90.31515
95.20845	55.43886	75.00357	93.70288
97.25029	56.46374	79.98648	96.95277
99.27105	57.48342	84.98993	100.12592
101.32859	58.50113	90.006	103.1441
		94.98096	106.05581
<b>Absolute Pressure (kPa)</b>	<b>Gas Uptake (cm<sup>3</sup>/g)</b>	99.98436	108.9372
<b>C<sub>2</sub>H<sub>4</sub> (298 K)</b>			
0.0042	0.01781	<b>Absolute Pressure (kPa)</b>	<b>Gas Uptake (cm<sup>3</sup>/g)</b>
1.31182	4.27301	<b>C<sub>2</sub>H<sub>6</sub> (298 K)</b>	
1.62571	5.25013	3.90455	7.09556
1.83905	5.76851	6.56122	11.38256
2.07207	6.49743	8.9793	15.00554
2.48161	7.57684	11.5738	18.60925
2.83028	8.4338	14.1169	21.98117
3.26806	9.56724	16.68022	25.19314

3.81959	10.88686	19.2316	28.24078
4.41075	12.3059	21.80673	31.16959
5.16233	13.94174	24.70023	34.35548
5.94384	15.66399	26.93109	36.70863
6.94263	17.74532	29.83347	39.67665
8.027	19.88337	32.41556	42.2532
9.3164	22.28511	35.07772	44.83561
10.806	24.90814	37.63598	47.25602
12.55931	27.77958	40.14906	49.58628
14.55165	30.82379	42.49478	51.70804
16.92014	34.14959	45.17522	54.03851
19.61622	37.61099	47.69923	56.17755
22.7768	41.33	50.29505	58.32796
26.4408	45.26028	52.94006	60.45315
30.69292	49.41032	55.51495	62.46409
35.62816	53.7789	57.98895	64.35459
41.352	58.38875	60.34116	66.08235
48.01624	63.26293	63.10914	68.0744
55.73729	68.41573	65.84576	69.98045
64.72002	73.88714	68.26399	71.64638
75.10816	80.18933	70.85633	73.37033
87.55251	86.35233	73.39629	75.0125
101.19379	92.51442	76.057	76.6779
		78.35977	78.10772
<b>Absolute Pressure (kPa)</b>	<b>Gas Uptake (cm<sup>3</sup>/g)</b>	81.00205	79.67945
<b>C<sub>3</sub>H<sub>4</sub> (298 K)</b>		83.55448	81.17112
0.12707	16.2673	85.89868	82.49029
1.5589	51.34005	88.80617	84.10239
3.03559	69.0871	91.29746	85.44902
4.45901	82.13961	93.9071	86.83721
5.99647	91.94463	96.24126	88.05017
7.73462	102.97833	99.0882	89.48321
9.06525	109.88841	101.68951	90.77801
10.32641	115.62938		
11.83102	121.79092	<b>Absolute Pressure (kPa)</b>	<b>Gas Uptake (cm<sup>3</sup>/g)</b>
13.34945	127.39158	<b>C<sub>3</sub>H<sub>4</sub> (273 K)</b>	
14.06411	130.15222	1.30913	77.18518
16.69583	138.56345	3.73753	121.30295
19.15885	145.54918	6.52395	147.53893
21.81166	152.30966	8.89255	163.72939
24.36046	158.23368	11.32543	176.49005

26.94277	163.65027	13.96859	187.92155
29.48207	168.59199	16.6252	197.62905
32.14952	173.44496	19.24954	205.97771
34.71476	177.68986	21.77567	213.12772
37.15589	181.53265	24.35756	219.65535
39.84973	185.49565	26.91935	225.52409
42.38555	189.03593	29.47351	230.98316
44.97649	192.49449	32.07378	236.11948
47.52889	195.75326	34.63318	240.7618
50.08356	198.84425	37.27182	245.19499
52.63886	201.81785	39.86174	249.10608
55.22037	204.70917	42.37242	252.60454
57.77403	207.44396	44.95282	256.04485
60.34329	210.10997	47.5117	259.3673
62.90193	212.6283	50.07652	262.70818
65.46119	215.12928	52.60646	266.14047
68.03261	217.53076	55.15723	270.10508
70.59674	219.85506	57.68055	275.24533
73.15749	222.06498	60.09383	283.10929
75.70466	224.25723	62.99327	294.54949
78.30255	226.4425	66.28928	301.7559
80.86044	228.50019	69.39068	304.9735
83.40937	230.51304	72.05426	307.23018
85.97916	232.47853	73.04844	308.16482
88.53953	234.39744	75.89679	309.91195
91.05092	236.20948	78.20897	310.83149
93.67022	238.09599	80.77892	311.68224
96.23823	239.87498	83.39706	312.50649
98.71228	241.52575	85.97817	313.27854
101.36088	243.24673	88.54039	313.97679
		91.09518	314.67099
<b>Absolute Pressure (kPa)</b>	<b>Gas Uptake (cm<sup>3</sup>/g)</b>	93.68078	315.36402
<b>C<sub>3</sub>H<sub>6</sub> (298 K)</b>		96.21932	316.01138
1.39359	30.11626	98.73722	316.62358
4.05796	53.63365	101.35639	317.26027
6.23123	65.8203		
9.44782	79.40907	<b>Absolute Pressure (kPa)</b>	<b>Gas Uptake (cm<sup>3</sup>/g)</b>
11.3066	85.58158	<b>C<sub>3</sub>H<sub>6</sub> (273 K)</b>	
13.9851	93.18771	1.30428	55.31028
16.69133	99.67072	3.89534	92.53348
19.17897	105.05022	6.99825	115.68258

21.90183	110.21373	9.48677	127.71594
24.40918	114.46453	11.29324	135.39388
26.9121	118.33471	14.21694	145.09627
29.57563	122.07077	16.63787	151.77251
32.05701	125.27951	19.25261	157.97714
34.67892	128.51216	21.83264	163.32273
37.27579	131.42308	24.38757	168.17305
39.82111	134.05823	26.97567	172.59815
42.36268	136.643	29.52145	176.70214
44.95807	139.13267	32.10582	180.52058
47.51452	141.47479	34.65281	184.10463
50.10427	143.75542	37.22854	187.5291
52.65937	145.88774	39.78718	190.78215
55.19363	147.95007	42.35807	193.87974
57.79863	149.95295	44.92001	196.7829
60.31668	151.80605	47.47412	199.58111
62.90713	153.66207	50.04509	202.32488
65.47921	155.45103	52.61518	204.88836
68.01684	157.16358	55.16695	207.34753
70.60026	158.85625	57.73535	209.78394
73.15982	160.43778	60.30037	212.14916
75.70459	162.00983	62.86747	214.43071
78.30671	163.5193	65.4244	216.6483
80.8201	164.99059	67.99307	218.76029
83.3814	166.44707	70.54932	220.82709
85.98639	167.9053	73.12041	222.88469
88.56399	169.26593	75.68207	224.85751
91.09941	170.59416	78.24212	226.72402
93.67316	171.95195	80.80174	228.55032
96.20202	173.21708	83.36967	230.33924
98.70595	174.44736	85.93465	232.09395
101.36966	175.71115	88.50328	233.73787
		91.05187	235.42746
<b>Absolute Pressure (kPa)</b>	<b>Gas Uptake (cm<sup>3</sup>/g)</b>	93.63546	237.05163
<b>C<sub>3</sub>H<sub>8</sub> (298 K)</b>		96.17935	238.65938
1.11001	13.56051	98.7561	240.22357
2.54651	26.89512	101.31261	241.72816
4.02196	38.6898		
6.63581	54.14039		
8.86241	63.61559		
11.33271	71.90591		
14.0506	79.19623		

16.58594	84.91785		
19.21624	90.045		
21.77966	94.47054		
24.37359	98.46281		
27.22407	102.41834		
29.74286	105.64111		
32.34977	108.76755		
34.9885	111.6956		
37.53511	114.37564		
40.06145	116.90063		
42.69152	119.40876		
45.18096	121.69172		
47.77955	123.97266		
50.28827	126.09869		
52.84106	128.17574		
55.47173	130.25015		
57.90819	132.12245		
60.59671	134.11524		
63.16222	135.97125		
65.6082	137.71293		
68.23492	139.51698		
70.77346	141.21175		
73.32704	142.89197		
75.9189	144.56062		
78.4451	146.15642		
81.13197	147.78692		
83.69229	149.33247		
86.13737	150.78197		
88.54692	152.16339		
91.28388	153.71361		
93.78496	155.10471		
96.17507	156.39113		
98.98563	157.87984		
101.56566	159.24087		

## References

1. D. S. Surry and S. L. Buchwald, *Chem. Sci.*, 2011, **2**, 27.
2. (a) G. M. Sheldrick, SHELXTL-NT, version 5.1; Bruker AXS Inc., Madison, WI, 1997; (b) O. V. Dolomanov, L. J. Bourhis, R. J. Gildea, J. A. K. Howard and H.

- Puschmann, *J. Appl. Crystallogr.*, 2009, **42**, 339.
3. V. A. Blatov, A. P. Shevchenko and D. M. Proserpio, *Cryst. Growth Des.*, 2014, **14**, 3576.
  4. L. Li, R.-B. Lin, R. Krishna, H. Li, S. Xiang, H. Wu, J. Li, W. Zhou and B. Chen, *Science*, 2018, **362**, 443.
  5. A. L. Myers and J. M. Prausnitz, *AIChE J.*, 1965, **11**, 121.
  6. A. K. Rappe, C. J. Casewit, K. S. Colwell, W. A. Goddard and W. M. Skiff, *J. Am. Chem. Soc.*, 1992, **114**, 10024.
  7. R. Stryjek and J. H. Vera, *Can. J. Chem. Eng.*, 1986, **64**, 323.
  8. B. Delley, *J. Chem. Phys.*, 2000, **113**, 7756.
  9. Z. Bao, S. Alnemrat, L. Yu, I. Vasiliev, Q. Ren, X. Lu and S. Deng, *Langmuir*, 2011, **27**, 13554.
  10. S. Plimpton, *J. Comput. Phys.*, 1995, **117**, 1.
  11. W. G. Hoover, *Phys. Rev. A*, 1985, **31**, 1695.
  12. S. Nosé, *J. Chem. Phys.*, 1984, **81**, 511.
  13. M. P. Allen and D. J. Tildesley, *Oxford: Clarendon Press*, 1987.
  14. P. S. Crozier, R. L. Rowley and D. Henderson, *J. Chem. Phys.*, 2001, **114**, 7513.
  15. X. Wang, R. Krishna, L. Li, B. Wang, T. He, Y.-Z. Zhang, J.-R. Li and J. Li, *Chem. Eng. J.*, 2018, **346**, 489.